Geologica Acta, Vol.6, Nº 4, December 2008, 293-312
DOI: 10.1344/105.000000258
Available online at www.geologica-acta.com

geologica acta

Tectono-metamorphic evolution of the Wadi Hafafit Culmination (central Eastern Desert, Egypt). Implication for Neoproterozoic core complex exhumation in NE Africa

H. ABD EL-NABY [1, 2,*] **W. FRISCH** [2] **and W. SIEBEL** [2]

[1] **Nuclear Materials Authority**
P.O. 530 El-Maadi, Cairo, Egypt

[2] **Institut für Geowissenschaften, Universität Tübingen**
Sigwartstr. 10, D-72076 Tübingen, Germany

[*] Corresponding author. Present address: **King Abdulaziz University, Faculty of Earth Sciences.**
P.O. Box 80206 Jeddah 21589. E-mail: hhabdel@yahoo.com

ABSTRACT

The Neoproterozoic rock assemblages in the Wadi Hafafit Culmination (WHC) can be subdivided into two main units which are separated by the Nugrus Thrust. The structurally higher Nugrus unit is mainly composed of low grade micaschists, metavolcanic, serpentinites, and metagabbros. The overthrusted Hafafit unit forms the Hafafit domes and is composed of ortho- and para-gneisses associated with amphibolite and ultramafic rocks. Mineral chemistry and thermobarometry indicate that the WHC was affected by two main metamorphic phases. The first metamorphic phase (M1), observed in the micaschists of the Nugrus unit, is characterized by greenschist-facies conditions. Garnet-biotite and garnet-muscovite geothermometry, as well as temperatures calculated by means of the TWEEQU program yield temperatures of 400°–550°C, whereas the white mica geobarometer reveals pressure of 3.7-4.9 kbar for this metamorphic phase (M1). The second metamorphic phase (M2), observed in gneisses and amphibolites of the Hafafit unit, is characterized by amphibolite-facies conditions. Garnet-biotite, garnet-amphibole and amphibole-plagioclase geothermometry yield temperatures of 600°–750°C, whereas the garnet-hornblende-plagioclase-quartz geobarometer indicates pressures of 6-8 kbar for the second metamorphic phase (M2). Sm-Nd and Rb-Sr whole rock-mineral isochron ages around 590 Ma for gneisses and amphibolites probably represent cooling from the metamorphic thermal peak which was attained around 600 Ma or slightly earlier. A 3-stage geologic evolution model is proposed for the tectonic evolution of the WHC. The first stage started earlier than 680 Ma ago with rifting and ocean floor spreading at a time which is as yet unspecified. It was followed by a second stage of subduction and emplacement of subduction-related granitoids around 620-640 Ma. At this time, the Hafafit region has become an active margin with the production of large amounts of calc-alkaline subduction-related volcanic and plutonic sequences. Subduction was terminated by collision and NW-ward Nugrus Nappe thrusting under greenschist-facies conditions (M1) around 620-640 Ma. At this stage, rocks of Hafafit unit were subjected to intense deformation and metamorphism in amphibolite facies (M2). Next came the third stage of late-orogenic extension and crustal thinning that was controlled by the Najd transform faults (620-580 my) and that resulted in exhumation of the Hafafit domes through a combination of transpression and lateral extrusion.

KEYWORDS | **Precambrian. Subduction. Metamorphism. Thermobarometry. Radiometric age dating.**

INTRODUCTION

The Egyptian Eastern Desert, Sudan, western Saudi Arabia, Ethiopia, Eritrea, Jordan and Yemen belong to the so-called Arabian Nubian Shield (Fig. 1), which is characterized by four main rock sequences: (i) an island arc assemblage; (ii) an ophiolite assemblage; (iii) a gneiss assemblage that comprises the core complexes; and (iv) granitoid intrusions (Abdel Naby et al., 2000; Abd El-Naby and Frisch, 2002). The core complexes and the major tectonic trend on both sides of the Red Sea strike northwest–southeast (Fig. 1) and are related to a crustal-scale sinistral shear zone called the Najd Fault System (Stern, 1985).

A series of medium- to high-grade core complexes have been recognized in the central and southern Eastern Desert of Egypt. They are surrounded by low-grade volcano-sedimentary nappes of Neoproterozoic age (Fritz et al., 1996, 2002). The most widely recognized basement domes are the Meatiq, the Sibai and the Hafafit domes (Fig. 2A). These core complexes and the adjacent volcano-sedimentary rocks are related to northwestward propagating thrusts (Berhe, 1990). They have been linked to possible subduction and collision phases during the Neoproterozoic Pan-African orogeny (Stoeser and Camp, 1985; Abdelsalam and Stern, 1993). Similar core complexes have also been reported from the Wadi Kid area in Sinai (Blasband et al., 1997, 2000).

The Wadi Hafafit Culmination (WHC) consists of two main units which are separated by the Nugrus Thrust. The structurally higher Nugrus unit is mainly composed of low-grade ophiolitic melange and volcanic arc rocks (Bennett and Mosley, 1987). The underlying Hafafit unit consists of five granite-cored domes (domes A to E, Fig. 2C; Greiling et al., 1988). El Ramly et al. (1984) interpreted the Hafafit gneisses, the associated granitic cores and the Wadi Ghadir melange at the north-eastern part of the mapped area (Fig. 2B), as a result of Pan-African convergence and subduction of a marginal ocean basin. Rb-Sr and K-Ar cooling ages of 620 Ma on mica separated from migmatitic segregations of the psammitic gneisses of the WHC have been reported by Hashad et al. (1981). The granitic gneisses in the core of the WHC were earlier regarded as pre-Pan-African basement because of their complex metamorphic and structural history (e.g. El Gaby et al., 1984, 1988). However, Stern and Hedge (1985) obtained U-Pb dates on zircon of 682 Ma for the granitic core that intrudes the Hafafit gneisses, which they interpreted as being of crystallization age. On the other hand, Fritz et al. (2002) reported $^{40}Ar/^{39}Ar$ ages of 586 Ma for hornblende separated from the granitic core of the Hafafit domes. They interpreted these ages as cooling ages below 500°C associated with exhumation of WHC along localised NE-trending extensional faults.

In general, there is a number of mechanisms and models or combinations of two or more of them that have

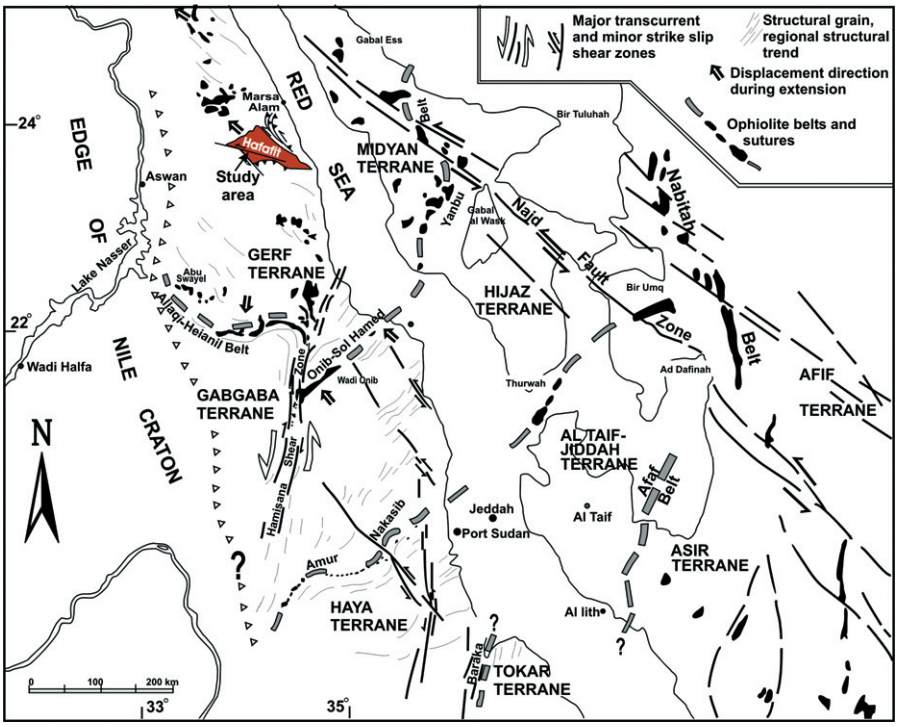

FIGURE 1 | **Schematic tectonic map of the Arabian Nubian Shield showing ophiolite belts, major structures and lineaments (Kröner et al., 1992). Tectonic elements in the Wadi Hafafit Culmination (WHC) were defined by Fritz et al. (1996). Major Tectonic units in Arabia after Camp (1984) and Johnson and Vranas (1984).**

been proposed for the origin of gneiss domes: (1) diapirism (Gans et al., 1989; Lister and Baldwin, 1993), (2) gravity collapse (Burchfiel and Royden, 1985; Blasband et al., 2000), (3) channel flow and ductile extrusion (Mancktelow, 1995; Beaumont et al., 2001), (4) compression and extension (Edwards et al., 1996; Davidson et al., 1997; Fritz et al., 2002), and (5) fold interference and large-scale sheath-folding (Fowler and El Kalioubi, 2002).

No quantitative data have been retrieved to characterize the metamorphism in the study area. Our data give a first quantification in this respect and show up clear differences in metamorphic grade, which is interpreted in terms of two metamorphic phases. We discuss field relations, petrography, mineral chemistry and thermobarometric data as well as Rb/Sr and Sm/Nd ages for rocks of WHC. These results are important for understanding the tectonometamorphic evolution of the WHC and add to the body of information about metamorphic core complexes in the Eastern Desert, their mode of formation and are critical to future modeling of the overall tectonic evolution of the Arabian-Nubian Shield.

GEOLOGICAL SETTING

Lithologically, the rock types in the Hafafit area consist of two main units that occur at spatially distinct subareas and are separated by the Nugrus Thrust (Fig. 2C). The overlying unit (Nugrus unit) is mainly made up of low grade micaschists and metavolcanics that outcrop in

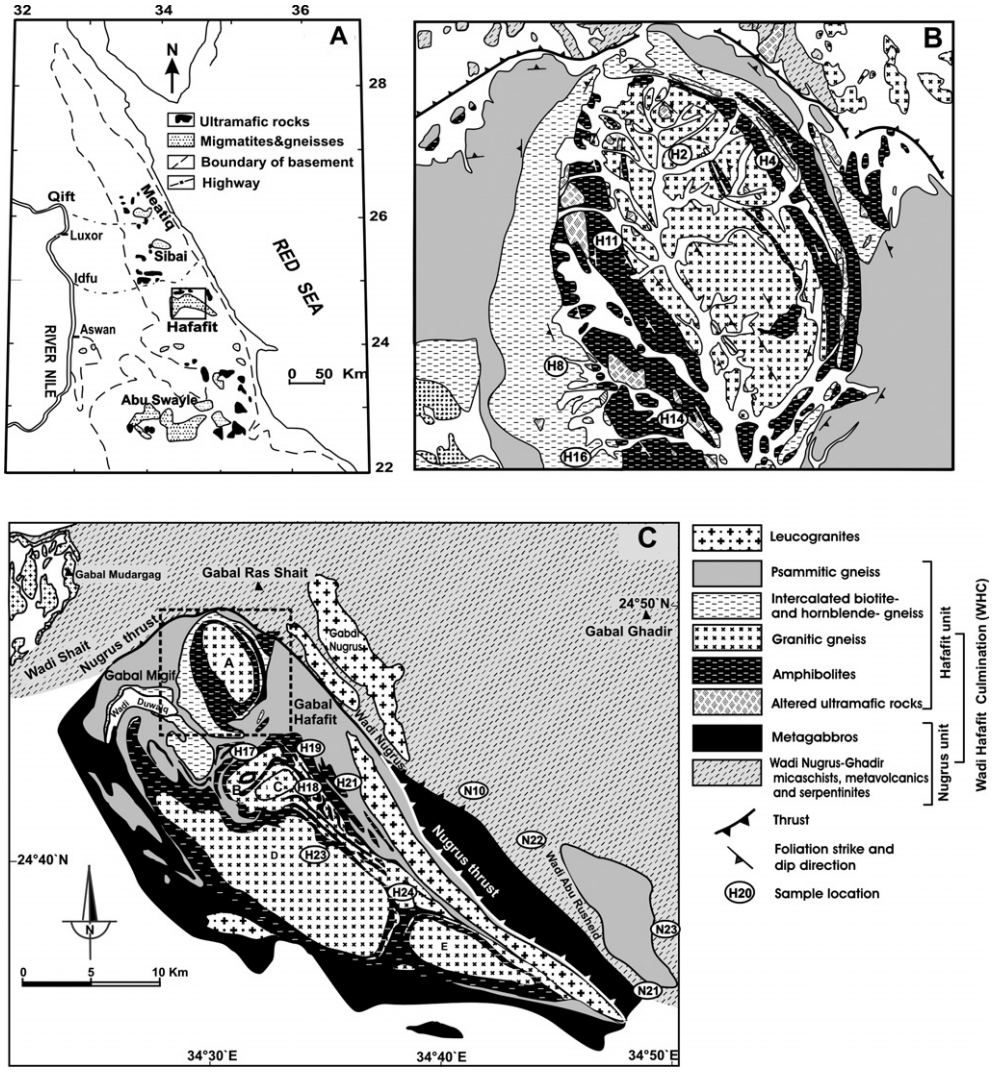

FIGURE 2 | **A) Location map of the study area. B) Detailed geological map of dome A (after El Ramly et al., 1993). C) General geological map of the study area (modified from El Ramly et al., 1993). Dashed square shows the position of Figure 2B.**

the eastern and northern part of the WHC. These rocks are associated with serpentinites and metagabbros. The metavolcanic rocks are exposed mainly at the northern and eastern border of the WHC. They are fine to medium grained meta-andesites which are porphyritic in some places. In the northern part of the mapped area (Fig. 2C), serpentinites form a conspicuous ridge of Gabal Ras Shait. Several other small serpentinite masses crop out to the east of Nugrus Thrust.

The underlying unit (Hafafit unit) is represented mainly by the Hafafit domes and consists of (from core to rim, Fig. 2B): granitic gneiss of tonalitic and trondhjemitic composition, banded amphibolite, altered ultramafic rocks, alternating bands of biotite- and hornblende-gneiss and psammitic gneiss at the rim of the domal structure. In some parts, the amphibolite is associated with metagabbro. Both units have been intruded by undeformed leucogranites, especially along thrust zones.

The granitic gneisses in the cores are coarse-grained and moderately foliated. The foliation is defined by flattened biotite-rich streaks and indistinct, elongated lithosomes of quartz and feldspar in the intervening felsic parts. The granitic gneisses show well-developed granoblastic-polygonal texture, and locally, mylonitic texture is observed in strongly deformed varieties. Two main types of granitic gneiss occur: predominant tonalitic gneiss and subordinate trondhjemitic gneiss. These rocks show a well-developed millimetre-spaced gneissic banding. In some places, the tonalites are invaded by numerous thin pegmatitic veinlets.

The amphibolites form irregular, lens-shaped bodies overthrusted by altered ultramafic rocks. At the southern part of dome A, the amphibolites are overlain by the psammitic gneiss of Gabal Hafafit. The contact between them is thought to be an initial preserved sedimentary one (Abd El-Naby and Frisch, 2006). The strong foliation of the amphibolites may be related to the first deformational event (El Ramly et al., 1993), which led to a metamorphic banding and may be synchronous with the formation of alternating bands of biotite- and hornblende-gneisses formed under amphibolite facies conditions. At the eastern side of the Nugrus Thrust, minor amphibolites occur in association with metagabbros, which probably belong to the group of calc-alkaline metagabbros associated with the Hafafit gneisses (El Ramly et al., 1993). Altered ultramafic rocks, mainly serpentinized dunite and pyroxenite, are found as small masses in the core of the northern Hafafit dome (dome A, Fig. 2B) overlying the amphibolites.

The alternating bands of biotite-gneiss and hornblende-gneiss are intercalated between the amphibolites and the psammitic gneiss. In Wadi Abu Rusheid, the psammitic gneiss is mylonitized and dissected by several shear zones. It exhibits extensive alteration, including silicification, sericitization, carbonatization and ferrugination. A secondary uranium mineralization is found in the altered zone of the mylonitic psammitic gneiss, where it occurs as stains along crevices and fracture surfaces and as acicular crystals filling cavities. Uranium and thorium contents vary from normal values to 55 and 225 ppm, respectively. Uranophane is the most abundant uranium mineral (Abd El-Naby and Frisch, 2006).

The latest Pan-African activity in the mapped area is represented by a suite of leucogranites and minor intrusions of felsite and aplite which intruded the Hafafit gneisses and the ophiolitic assemblage (El Ramly et al., 1993). Elongated narrow intrusive leucogranite is found parallel to the Nugrus Thrust (Fig. 2C). To the other side of the Nugrus Thrust, there is another elongated granitic belt forming Gabal Nugrus. Generally, these leucogranites are garnet-bearing, e.g. garnetiferous granites. Several small lens-like plutonic masses of leucogranites are found also in Wadi Abu Rusheid.

A structural evolutionary scheme involving eleven deformation phases (D1 to D11) in the WHC was presented by El Ramly et al. (1984) and Greiling et al. (1984). It was later grouped into four deformation stages (D1–D4; D5–D7; D8–D10; D11) by El Ramly et al. (1993), and subsequently modified to nine deformation phases (Greiling et al., 1994). These deformation phases led to a complex pattern of a series of anticlines and synclines, strike-slip and normal faults. Fowler and El Kalioubi (2002) stated that the Hafafit domes are a result of the interference of four macroscopic fold phases, the first three of which may represent a single deformational event. Table 1 (see p. 308) summarizes the sequence of structural events for the WHC, as proposed by Greiling et al. (1984), El Ramly et al. (1993), Greiling et al. (1994) and Fowler and El Kalioubi (2002).

PETROGRAPHY

Nugrus unit

The micaschist of the Nugrus unit is mostly composed of garnet, muscovite, biotite, quartz, plagioclase, chlorite, and ilmenite (Fig. 3A). Garnet is present as idiomorphic to subidiomorphic porphyroblasts with inclusions of quartz, muscovite, biotite, chlorite and ilmenite. In the matrix, biotite and muscovite occur as flakes, approximately 0.5 and 1.5 mm in length, respectively, which are partly oriented parallel to the main foliation coexisting with quartz, chlorite and garnet. Plagioclase is untwinned

and some show compositional zoning. Alteration to epidote and inclusions of ilmenite, biotite and quartz were observed. A small amount of retrogressive chlorite has been found in some samples. Ilmenite occurs as inclusion in garnet and along the foliation planes. Metavolcanic rocks include meta-basalt and meta-andesite. They are composed of hornblende or actinolite-tremolite and plagioclase (An_{43-50}). Retrograde partial replacement of hornblende by actinolite or tremolite and plagioclase by epidote and calcite is observed. Metagabbros are generally medium to coarse grained and consist of highly saussuritized plagioclase and hornblende which is partly altered to pale green actinolite and/or chlorite.

Hafafit unit

Less altered ultramafic rocks, found in the core of dome A (Fig. 2B), are composed mainly of olivine, which is widely replaced by serpentine forming the typical mesh texture (Fig. 3B), whereas highly altered samples consist of serpentine, talc, chlorite, tremolite and carbonate. The fine-grained amphibolites can be divided into three compositional groups based on their preserved mineral assemblages. Group 1 are clinopyroxene amphibolites, which consist of amphibole, clinopyroxene, plagioclase with little quartz and ilmenite. A few millimeters to one centimetre alternating bands are either dark grey, mainly of amphibole and plagioclase or dark green, mainly of clinopyroxene, respectively (Fig. 3C). In thin section, clinopyroxene is colourless to pale green (in Z direction) and varies in size from 0.2 to 2 mm. Some crystals are altered to bluish green hornblende. Group 2 are garnet amphibolites which consist of amphibole, plagioclase, garnet, quartz, ilmenite, but locally contains clinopyroxene (sample H17, Table 2, see p. 308). The garnet is coarse grained (up to 5 mm in diameter) and occurs throughout the rock as anhedral porphyroblasts that contain inclusions of quartz, amphibole and ilmenite. Group 3 are massive amphibolites, which lack both clinopyroxene and garnet, and occur as lenses within the gneisses. They are composed mainly of amphibole, plagioclase, quartz and ilmenite.

The tonalitic/trondhjemitic gneiss consists of plagioclase, quartz, biotite and, locally, garnet. Plagioclase forms subidiomorphic laths which show albite twinning in most cases. Biotite forms flakes up to 2 mm long which are partially aligned parallel to the foliation. Pleochroism is moderate, from light brown to greenish brown. Partial alteration of biotite to chlorite is common. Garnet is found as small xenomorphic to idiomorphic crystals with inclusions of quartz and plagioclase.

The biotite-gneiss is composed essentially of quartz, biotite and plagioclase. Garnet, observed in some samples, occurs as inclusion-rich xenomorphic crystal and generally shows embayed grain boundaries. The common

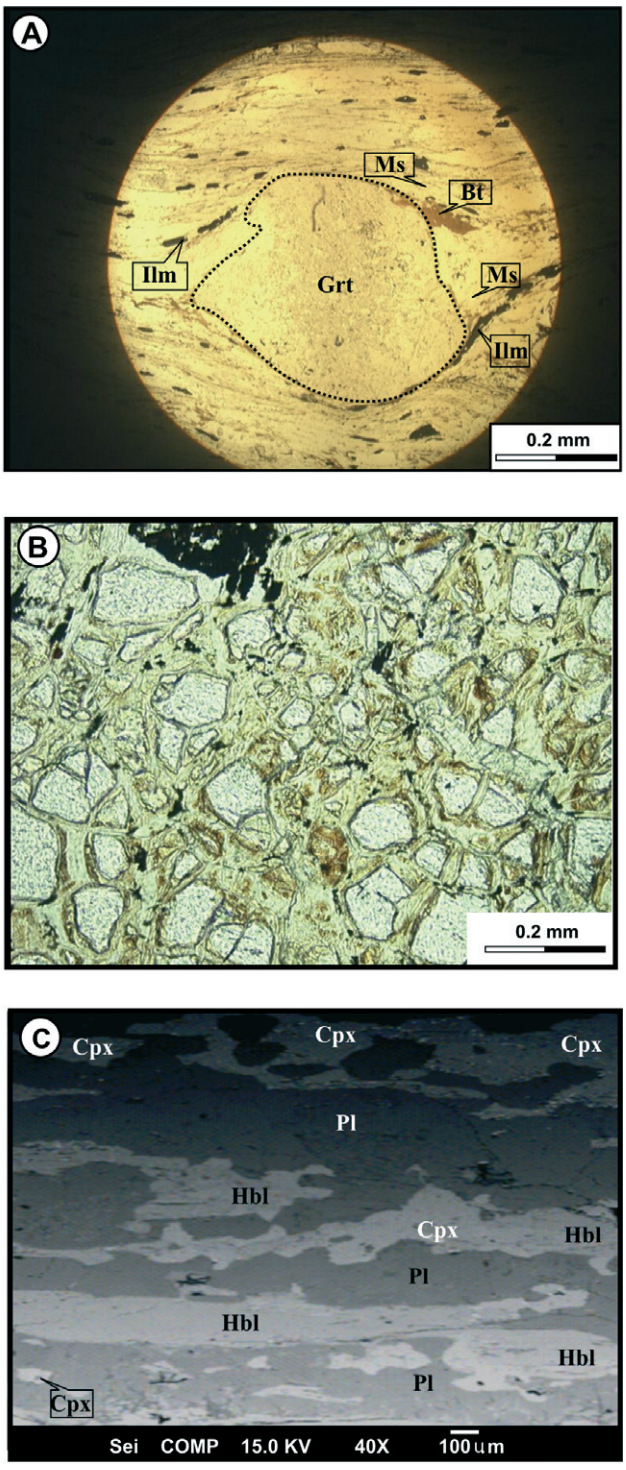

FIGURE 3 **A) Garnet porphyroblast in micaschist from the Nugrus area. Note the external foliation of muscovite and biotite wrapping around garnet. B) Less altered ultramafic rock showing relic olivine grains in a mesh texture of serpentine. C) Back scattered image showing alternation of amphibole-, plagioclase- and clinopyroxene–rich bands in clinopyroxene amphibolites. Mineral abbreviations are after Kretz (1983).**

occurrence of biotite inclusions suggests that garnet was formed by a biotite-consuming reaction. Chlorite and epidote are present as alteration phases in some samples. The hornblende-gneiss consists mainly of hornblende, plagioclase and quartz with some ilmenite. Hornblende occurs as aggregates of xenomorphic to subidiomorphic grains. Subordinate biotite is recorded in some thin sections. The psammitic gneiss forms the summits of the major mountains in the area (e.g. Gabal Hafafit and Gabal Migif). It is essentially composed of quartz, K-feldspar, plagioclase, and minor amphibole, biotite and epidote. The sedimentary origin of these gneisses in a back-arc basin is indicated from their geochemical characteristics (Abd El-Naby and Frisch, 2006). Leucogranites are medium to coarse-grained; they predominantly consist of quartz, plagioclase and K-feldspar and contain small amounts of biotite, muscovite and garnet. Garnet is ubiquitous and occurs as equigranular euhedral grains containing few mineral inclusions. Muscovite commonly shows poikilitic texture indicating late-stage crystallization.

MINERAL CHEMISTRY

From the 50 samples of the different rock types studied, 15 were selected for mineral analyses using a JEOL JXA-8900RL instrument at the Institute of Geosciences, University of Tübingen, Germany. Analytical conditions were 15 kV accelerating voltage, 10–20 nA beam current, 1–2 μm beam diameter and 10–20 seconds counting time. Electron microprobe analyses were carried out on amphibole, plagioclase, garnet, clinopyroxene, biotite, chlorite and muscovite from the amphibolites, biotite-hornblende gneisses and micaschists. The mineral compositions are used to constrain the metamorphic conditions which occurred during mineral formation using suitable thermobarometric calculation. Table 2 (see p. 308) shows a summary of the mineral assemblages, whereas representative analyses of these minerals and their chemical formula are listed in Tables 3 to 8, (see p. 309-311).

Amphibole in hornblende-gneiss and amphibolite is mainly magnesiohornblende (Table 3, Fig. 4), with the exception of the clinopyroxene amphibolite sample H21 which contains a magnesio-hastingsite and edenite, following the nomenclature of Leake et al. (1997).

Plagioclase (Table 4, see p. 309) shows a general increase in anorthite content from the micaschists (An_{14-17}) over the biotite- and hornblende gneisses (An_{16-42}) to the amphibolites (An_{35-76}) (Fig. 5A). However, in individual samples, the range is much smaller and does not exceed 5 mol% in micaschists and 10 mol% in biotite and hornblende gneisses and amphibolites. The plagioclase grains are either unzoned or show weak oscillatory zoning. An increase in An-content of grains in contact with garnet appears to be related to the depletion of X_{grs} [=Ca/(Fe+Mg+Mn+Ca)] in micaschists, whereas in amphibolites, such an increase is related to the plagioclase rims in contact with amphibole.

Garnet of the amphibolites, biotite-gneisses and micaschists is almandine-rich and X_{Alm} [Fe/(Fe+Mg +Mn+Ca)] varies from 53.3 to 93.6 mole % (Table 5, see p. 310; Fig. 5B). Microprobe profiles across garnet from a micaschist sample shows a virtually slight compositional zoning with a core richer in almandine and pyrope, and poorer in grossularite and spessartite (Fig. 6) than in amphibolite and gneisses. Most garnet from the studied rocks contains inclusions of quartz and ilmenite. However, evidence of rotation during growth is shown only in some of the micaschist samples (Fig. 3A).

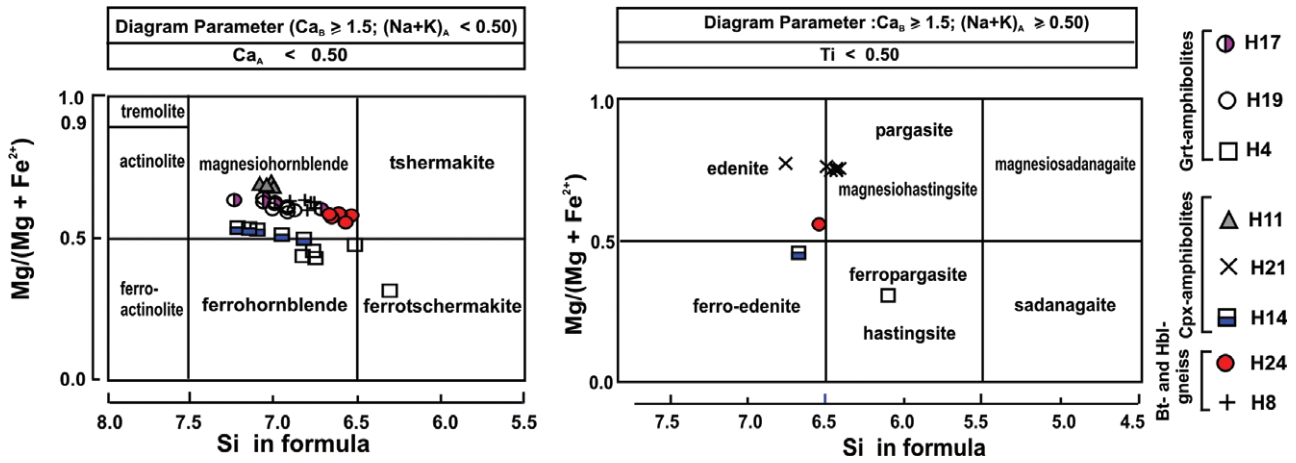

FIGURE 4 | **Composition of amphiboles from hornblende-gneisses and amphibolites plotted in the nomenclature diagram after Leake et al. (1997).**

Clinopyroxene (Table 6, see p. 310), found mainly in the clinopyroxene amphibolites, is associated with garnet in some places. It is diopside with Fe/(Fe+Mg) ranging from 0.195 to 0.220, the maximum Na_2O content being 0.24 wt.%. X_{Mg} =Mg/(Mg+Fe) of biotite (Table 7, see p. 310) ranges from 0.18 to 0.44 and 0.47 to 0.51 in micaschists of the Nugrus unit and the granitic gneisses of the Hafafit unit, respectively. The biotite in the micaschist is more titaniferous (1.5-2.9 wt.-% TiO_2) than in the biotite gneiss (0.01-0.62 wt.-% TiO_2). Based on the classification of Hey (1954), the chlorite (Table 8, see p. 311) from the micaschist has the composition of rhipidolite and pycnochlorite. The Si contents of muscovite (Table 8) in the micaschist vary from 6.51 to 6.61 per formula unit.

GEOTHERMOBAROMETRY

The diagnostic phases of most micaschists (garnet, biotite, muscovite, plagioclase, quartz and ± chlorite) suggest that the rocks have been metamorphosed up to the upper greenschist/lower amphibolite facies transition. The biotite and muscovite could be formed from the following reaction

$$3\ Chl + 8\ Kfs = 5\ Ann + 3\ Ms + 9\ Qtz + 4\ H_2O, \quad (1)$$

this reaction replaces the sedimentary assemblage K-feldspar + chlorite by biotite and muscovite (Fig. 7). The reaction affects rocks with low X_{Al} that do not contain pyrophyllite, where the first prograde biotite appears at about 420°C (Bucher and Fry, 1994). The garnet could be formed by the following reaction

$$1\ Ms + 3\ Chl + 3\ Qtz = 4\ Alm + 1\ Ann + 12\ H_2O \quad (2)$$

according to Bucher and Fry (1994), the equilibrium temperature for this reaction is approximately 540°C, where the mineral assemblage muscovite + chlorite + quartz are replaced by garnet and biotite (Fig. 7).

A basic assumption for geothermobarometry is that a mineral assemblage formed in equilibrium, but it is impossible to prove that minerals in an individual metamorphic rock ever achieved equilibrium. Therefore, care has to be taken in selecting the appropriate phases for electron microprobe analysis by choosing sharp grain boundaries and direct contacts. The garnet-biotite geo-

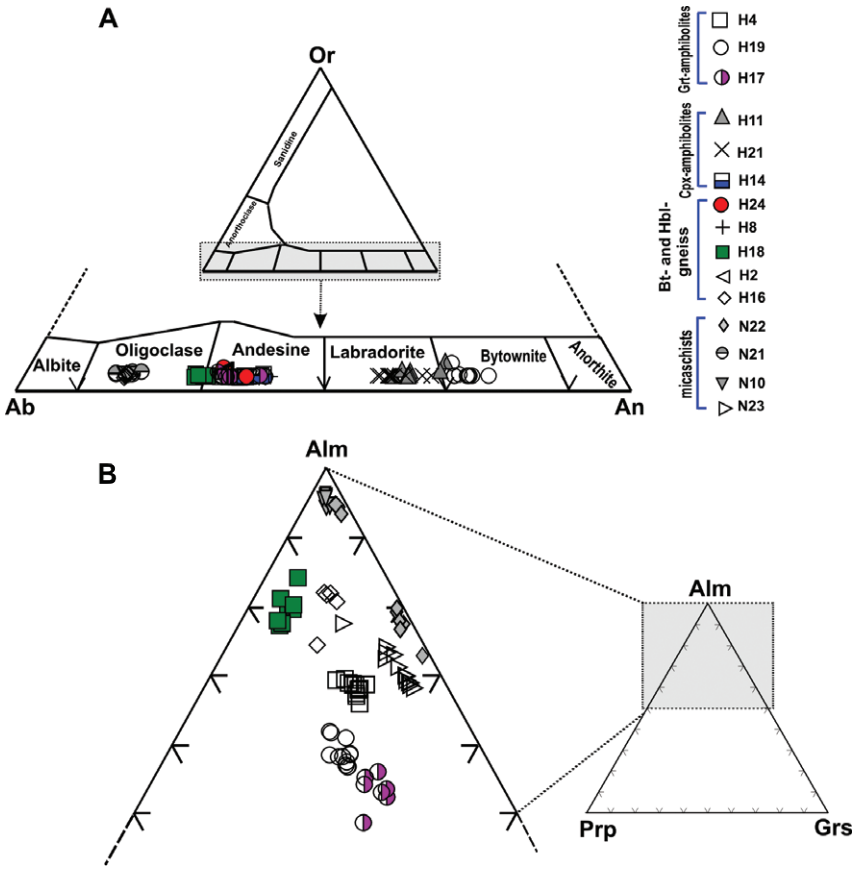

FIGURE 5 | **(A) Plagioclase composition. Note the increase in anorthite contents from micaschists, biotite- and hornblende-gneisses to amphibolites, presumably reflecting differences in bulk-rock composition. (B) Garnet composition of amphibolites, biotite-gneiss and micaschists. Or: orthoclase; Ab: albite; An: anorthite; Alm: almandine; Prp: pyrope; Grs: grossular.**

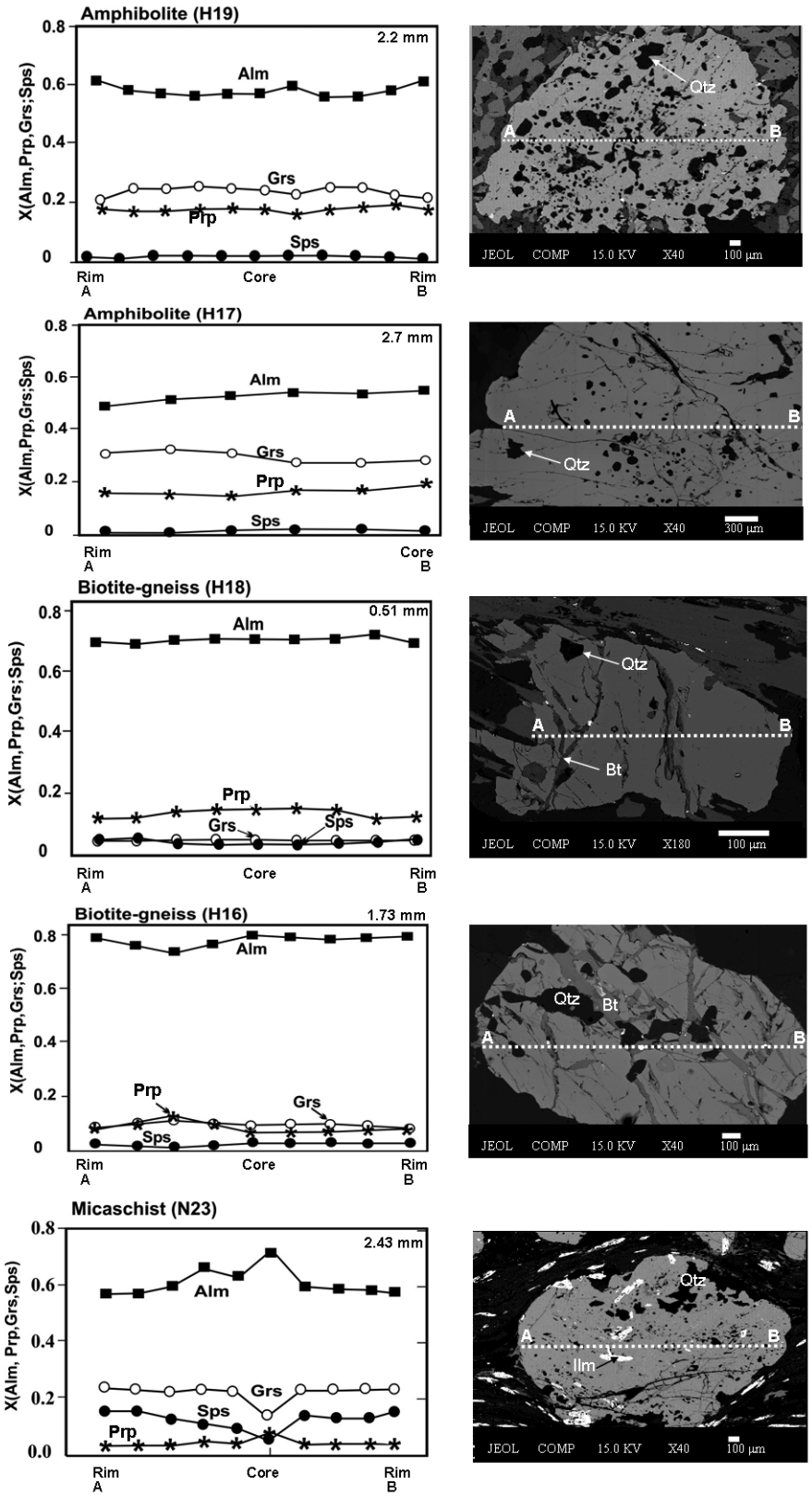

FIGURE 6 | **Representative garnet zoning profiles in amphibolite, biotite-gneiss and micaschist. Garnet of mica schist is slightly zoned than in amphibolite and gneiss. Back-scattered electron images of the analyzed garnets are shown for comparison. Alm: almandine; Prp: pyrope; Grs: grossular.**

thermometer after Ferry and Spear (1978), Hodges and Spear (1982), Bhattacharya et al. (1992) and Kleemann and Reinhardt (1994) was used for the biotite-gneiss sample H18 and the micaschist samples N10 and N23. The biotite-gneiss shows consistently higher temperatures (598°-686°C) than the micaschist (405°-550°C; Table 9, see p. 311). Temperatures for the micaschists (samples N10, N23, N22) were also calculated using the garnet-muscovite geothermometer of Hynes and Forest (1988). They yield temperatures between 400° and 527°C. These temperatures are close to those obtained from the garnet-biotite pairs. Grt–Ms-An-Bt phase equilibria were calculated with TWEEQU-program of Berman (1991) for the micaschist samples N10 and N23, yielding temperatures between 465° and 550°C (Table 9).

The phengite component of white mica is used as a pressure indicator (Velde, 1967; Guidotti and Sassi, 1976; Ernst, 1988), which was calibrated by Massonne and Schreyer (1987) as a barometer for quartz + biotite + white mica + K-feldspar assemblages. White mica from the micaschist samples N10, N23, and N22 yielded Si contents of 6.32 – 6.46 apfu corresponding to a pressure range of 3.5 to 5.7 kbar (at T = 450°C) and 4.3 to 6.4 kbar (at T = 500°C). Due to the absence of K-feldspar in the micaschist samples, the calculated pressures represent the minimum values.

Temperatures were calculated from coexisting amphibole and plagioclase pairs in the amphibolites and hornblende-gneisses following the formulation of Holland and Blundy (1994). The calculated temperatures are similar in the hornblende-gneisses and amphibolites (660-730°C, 635-750°C, respectively; accuracy ± 75°C; Table 9). Temperatures calculated from coexisting garnet and amphibole pairs for the garnet amphibolites using the calibration of Graham and Powell (1984) are 600-750°C (± 60°C; Table 9).

For the garnet amphibolites, pressures were calculated using the garnet-hornblende-plagioclase-quartz geobarometer (Kohn and Spear, 1990). Pressures estimated for sample H19, in conjunction with the temperatures given above (600-750°C), vary from 6.0 to 6.5 kbar (Table 9), with an accuracy of ±1 kbar, whereas sample H17 yields a pressure of 7.6-8.0 kbar and sample H4 of 6.5-7.6 kbar. P-T diagram showing the range of the estimated P-T condition of metamorphism of the metamorphic rocks of the WHC is shown in Fig. 7.

SM-ND AND Rb-Sr ISOTOPIC DATA

In order to constrain the timing of the metamorphic event, three samples from the Hafafit unit (biotite-gneiss H18, hornblende-gneiss H23 and amphibolite H19) were selected for age determinations. For Sm-Nd isotope analyses, samples were spiked with a mixed ^{149}Sm-^{150}Nd tracer solution. Plagioclase was dissolved in 52% HF for four days at 120°C on a hot plate. Whole-rock and garnet were digested in 52% HF for seven days at 180°C in a Teflon bomb surrounded by a steel jacket. Before digestion, garnets were leached in 9 N HCl for one hour at 80°C. For Rb-Sr isotope analyses samples were spiked with a mixed ^{84}Sr-^{87}Rb tracer solution and dissolved in 52% HF for four days at 120°C on a hot plate. All samples were dried and re-dissolved in 6N HCl, dried again and re-dissolved in 2.5N HCl. Rb, Sr, Sm and Nd were separated using conventional chromatographic procedures. All isotopic measurements were made by Thermal Ionization Mass Spectrometry, on a Finnigan MAT 262 mass spectrometer at the Institute of Geosciences, University of Tübingen, Germany. The La Jolla Nd-Standard yielded a value of 0.511815 ± 0.000009 (reference value 0.511850) whereas the NBS 987 Sr standard gave a $^{87}Sr/^{86}Sr$ ratio of 0.710254 ± 0.000009 (reference value 0.710248). Blanks for Sm and Nd were less than 40 pg and those for Rb and Sr less than 60 pg. The two-error regression method of Wendt (1986) was used for isochron calculation.

Sm-Nd isotopic data from garnet, plagioclase, and whole rock were used to date the metamorphism of the hornblende-gneiss sample H23 and the amphibolite H19 (Fig. 8, Table 10, see p. 312). The ages of 593 ± 4 and 585 ± 8 Ma, respectively, are identical within error. Moreover, a similar temperature (600°-750°C) for these rocks is indicated from the thermobarometric data.

Considering the closure temperature for the Sm-Nd system which may be around 600°C (Mezger et al., 1992) and the peak temperature estimate for sample H19 (600°-690°C), we conclude that the ages reflect the onset of cooling from the thermal peak. This conclusion agrees with the age data of Moghazi et al. (2004), who obtained Rb-Sr whole rock ages around 600 Ma for lens-shaped leucogranite bodies along thrust faults in the Sikait-Nugrus area, east of the WHC. They interpreted this age as the time of intrusion of the leucogranite or as the time of the high-temperature metamorphic overprint.

The biotite gneiss sample H18 yields a Rb-Sr biotite-whole rock-plagioclase isochron age of 573 ± 6 Ma. This age is slightly younger than the Sm-Nd ages (593 ± 4 and 585 ± 8 Ma) and may reflect a later stage in the cooling history than the Sm-Nd ages, as the closure temperature of the Rb-Sr system is at about 350°C for biotite. The present data agree with the ^{40}Ar-^{39}Ar ages obtained by Fritz et al. (2002) for hornblende separates from the Hafafit gneisses (~585 Ma).

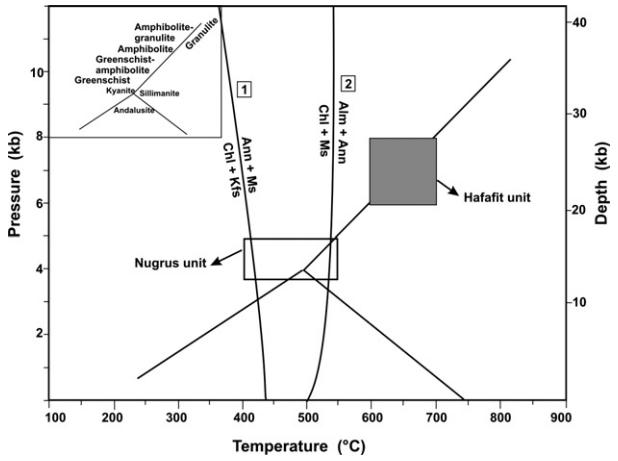

FIGURE 7 | **Pressure-temperature diagram showing the estimated P-T conditions of metamorphism for the rocks of the Wadi Hafafit Culmination. Curves 1 and 2 are reaction curves for pelitic rocks in the FASH system that defines biotite-in and garnet-in reactions, respectively (after Bucher and Frey, 1994).**

DISCUSSION

Three main mechanisms have been proposed to explain exhumation of core complexes within Egyptian Eastern Desert and Sinai. These include processes related to: 1) Diapiric intrusion as suggested by El Ramly et al. (1984) and Greiling et al. (1984) for the Hafafit gneiss domes, (2) gravity collapse as suggested by Blasband et al. (2000) for the Wadi Kid gneiss domes, and (3) compression and extension as suggested by Loizenbauer et al. (1999) and Fritz et al. (2002) for the Meatiq gneiss dome, Eastern Desert of Egypt.

Based on the obtained thermobarometric and geochronological data, we will try to test the applicability of each of these mechanisms to the formation of WHC. El Ramly et al. (1984) and Greilling et al. (1984) suggested gravitative uplift of the Hafafit domes, where the central part of the domes is occupied by later intruded, less deformed granitoid material. Fowler and El Kalioubi (2002) disputed the gravitative uplift model as a component of the deformation history of the Hafafit domes. Alternatively, they concluded that the fold interference pattern shown by the gneiss-cored domes of the WHC is a result of refolding of early macroscopic sheath folds. The absence of undeformed granitic rocks in the core of the Hafafit domes argues against the gravitative uplift model as suggested by El Ramly et al. (1984) and Greilling et al. (1984). Moreover, diapiric intrusion should produce a more radial pattern of deformation, a situation which is not recognized in the WHC.

Metamorphic core complexes in an extensional setting are characterized by low-pressure/high-temperature metamorphism in their lower crustal sequence due to the intrusion of granitoids into thinned crust (Gans et al., 1989; Lister and Baldwin, 1993). The present pressure estimates for the lowest structural level of the WHC (i.e., the amphibolites) are 6-8 kb which reflects a depth of 20-25 km. These data contradict the model of an extensional setting during a gravitational collapse. Moreover, extensional collapse required magmatic heating to weaken the lower and middle crust. In fact, field occurrences of several leucogranites in the Hafafit region point to the relation between granite intrusion and thrusting (Fig. 2C), i.e., the role of magmatic activity could be restricted in facilitating the displacement along thrust zones, but not to the extent as to promote extensional collapse.

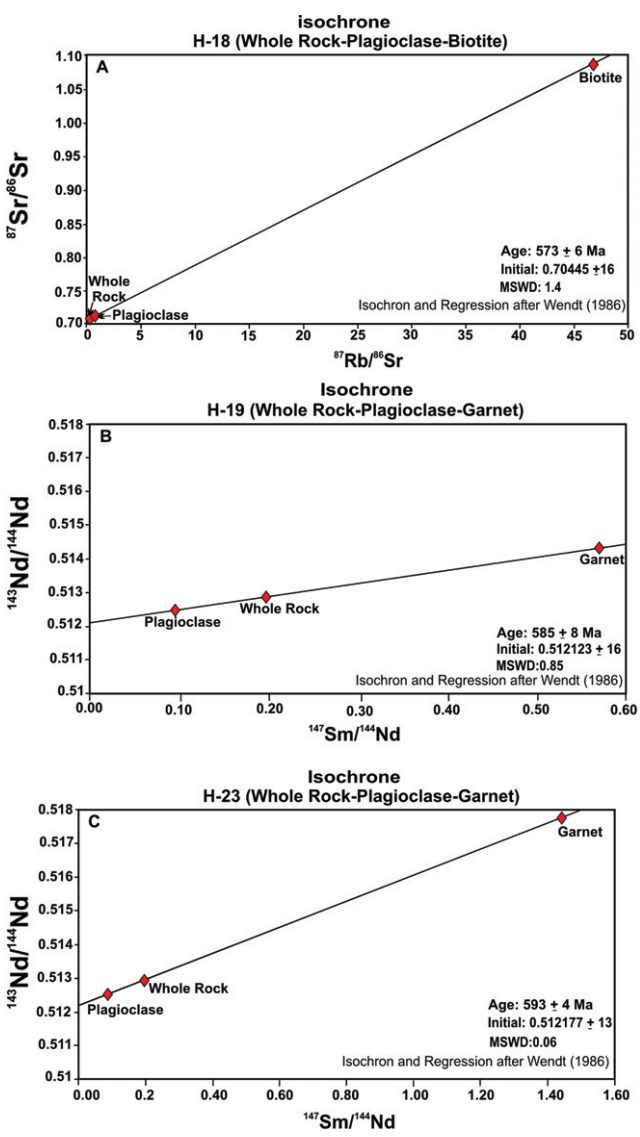

FIGURE 8 | **A, B and C) Isochron diagrams of Rb-Sr and Sm-Nd isotopic data.**

A combination of transpression and lateral extrusion model for the exhumation of the Hafafit domes is proposed by Fritz et al. (2002) where the bulk convergence is balanced by both vertical thickening and horizontal NW–SE directed extension. This model seems to be more applicable for three reasons: 1) The present Sm/Nd and Rb/Sr cooling ages (~590 Ma) are in accordance with the ^{40}Ar-^{39}Ar ages obtained by Fritz et al. (2002) for hornblende separates from the Hafafit gneisses (~585 Ma); 2) presence of both compressional and extensional structural styles in the WHC; and 3) emplacement of syn-extensional granitoids into the WHC as reported by Moghazi et al. (2004). Moreover, most previous works interpret the shear zones in the Hafafit area, which represent late-stage structures cutting across all earlier structures, as the result of an extensional event following continental collision, possibly related to the Najd Fault System.

Loizenbauer et al. (2001) and Fritz et al. (2002) divided the deformation events in the central Eastern Desert into three main phases. They suggested that the oldest observed deformation phase (D1) is related to the pre-Pan-African deformation and is only recognized in amphibolite enclaves within the core complexes. The D2 deformation is related to the Pan-African deformation associated with oblique convergence of the arc and back arc assemblage onto the Nile craton around 620–640 Ma (Fritz et al., 1996). The D3 deformation in the central Eastern Desert is characterized by the formation of crustal-scale NW–SE sinistral shear zones of the Najd Fault System (Stern, 1985; Loizenbauer et al., 2001) followed by exhumation of core complexes within orogen parallel extension around 620–580 Ma. The D4 deformation occurred much later and may be related to brittle deformation associated with the Red Sea rifting in Tertiary times.

P-T calculations using the various geothermobarometers on rocks from the WHC show two distinctly different sets of metamorphic conditions on either side of the Nugrus Thrust. The first is observed in the micaschists of the Nugrus unit to the northeast of the Nugrus Thrust, with a low-temperature-low-pressure assemblage, equilibrated between 400 and 550°C and between 3.7 and 4.9 kbar. The second, medium-temperature-medium-pressure assemblage equilibrated in the range 600-750°C at 6-8 kbar. This is observed in

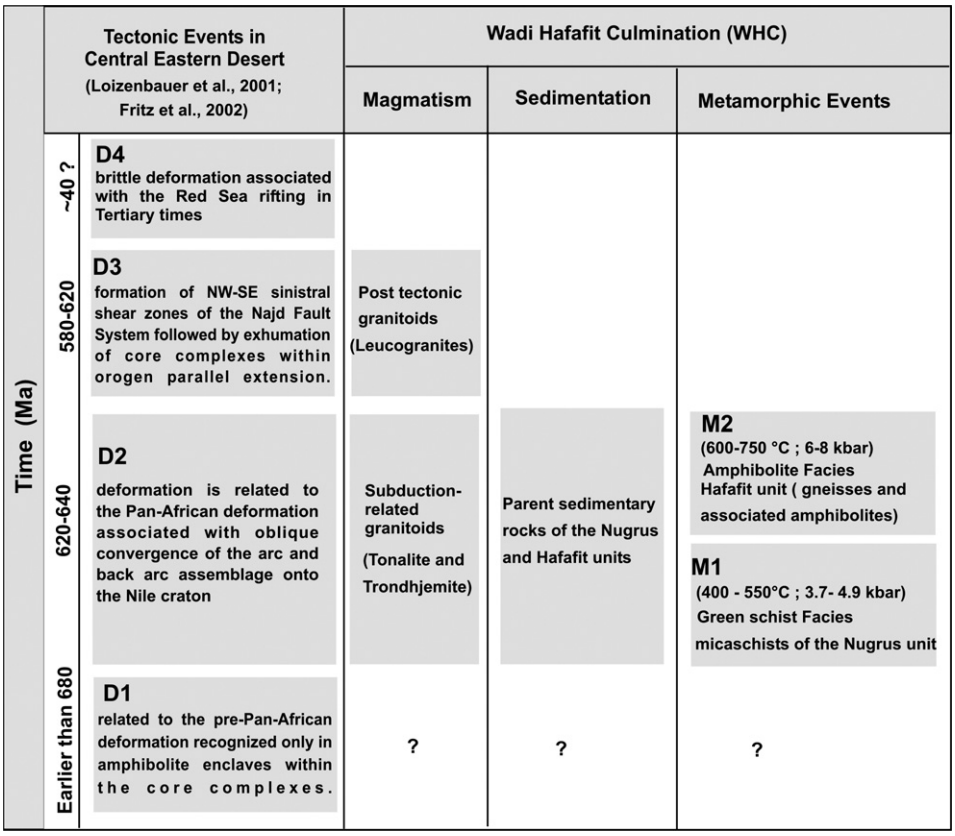

FIGURE 9 | **Relative timing of metamorphic events of the Wadi Hafafit Culmination (WHC) and their correlation with the tectonic events in the central Eastern Desert. See Figures 1 and 10 for location and further explanation of tectonic events and evolutionary stages.**

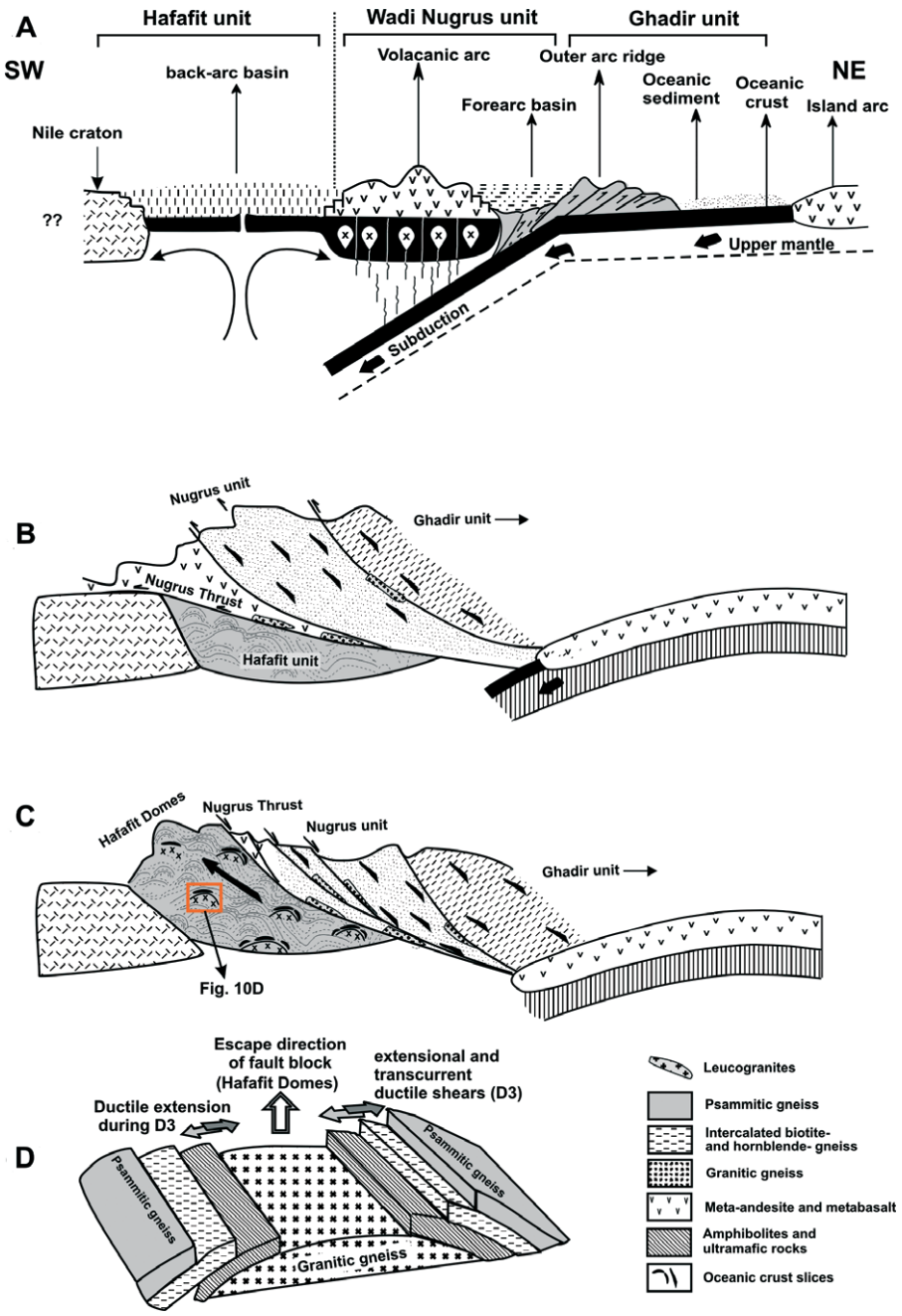

FIGURE 10 | **Sketch diagrams illustrating the possible geotectonic evolution of the Wadi Hafafit Culmination (modified from Abd El-Naby and Frisch, 2006). A) 620-640 Ma (D2 tectonic events): subduction of the oceanic crust, ophiolite detachment and thrusting in the Wadi Ghadir, with arc volcanism, arc-related plutonism and back-arc basin development in the Hafafit region. B) ~600 Ma (D3 tectonic events): NW vergent thrusting of Nugrus unit over Hafafit unit. C) 580-600 Ma (D3 tectonic events): exhumation of Hafafit domes by orogen parallel extension. (D) Close up view of one of Hafafit domes showing the extensional and transcurrent ductile shears associated with D3. See Figure 9 for further explanation of tectonic events.**

the Hafafit unit and represented by gneisses and associated amphibolites. The low-grade metamorphic phase, which is characterized by greenschist-facies conditions (Nugrus unit), is related to NW-ward Nugrus Nappe thrusting between 620-640 Ma (D2, Fig. 9). This event was responsible for metamorphic imprint on the sedimentary series of the Nugrus unit and could be assigned as "M1" (Fig. 9). This is consistent with the general conclusion of Neumayr et al. (1996, 1998) that the D2 deformation in the central Eastern Desert took place at greenschist facies conditions. At ~600 Ma or slightly earlier, rocks of the Hafafit unit were subjected to intense deformation and metamorphism in amphibolite facies (M2, Fig. 9). Moreover, the coincidence of

the emplacement age of the leucogranite (594 ± 12 and 610 ± 20 Ma; Moghazi et al., 2004) and the metamorphic ages (~600 Ma as deduced from the present study) of the Hafafit assemblages indicate that leucogranite generation and metamorphism of the Hafafit units are related to the same deformational event (late stage of D2, Fig. 9).

A 3-stage geologic evolution model is proposed for the tectonic evolution of the WHC. In this model, we adopted the idea of major extensional structures within overall compressive systems in mountain building processes. The rock assemblages of the Hafafit area correspond to accretion-collision units of island-arc and back-arc basin composition correlated to the subduction during Pan-African time (Fig. 10). The first stage started earlier than 680 Ma ago with rifting and ocean floor spreading at a time which is as yet unspecified. It corresponds to the D1 deformational event in the scheme of Loizenbauer et al. (2001) and Fritz et al. (2002). This stage was followed by a second stage of subduction and emplacement of subduction-related granitoids at ca. 682 Ma (Stern and Hedge, 1985). At this time, the Hafafit region has become an active margin with the production of large amounts of calc-alkaline subduction-related volcanic and plutonic sequences (Fig. 10A). This is in agreement with the chemistry of the granitic gneisses in the core of the Hafafit domes that correlated with arc-related granitoids (Abd El-Naby and Frisch, 2006). Remnants of the oceanic crust of the back-arc basin are represented by the amphibolites and ultramafic rocks found in the cores of Hafafit domes. The back-arc basin received sediments from the volcanic arc and the continent in the hinterland to the west (Nile Craton?).

Subduction and related calc-alkaline magmatism continued in the area for at least 80 Ma and was terminated by collision around 600 Ma. Collision was associated with NW-ward Nugrus Nappe thrusting under greenschist-facies conditions (M1). The back-arc basin sequence became buried to depth greater than 20 km (Fig. 10B). At this stage, rocks of Hafafit unit were subjected to intense deformation and metamorphism in amphibolite facies (M2). Subduction and collision stage corresponds to the D2 deformational event (Fig. 9). Next it came the third stage of late-orogenic extension and crustal thinning, which was controlled by the Najd transform faults. It gave exhumation of the Hafafit domes (Fig. 10C-D) through a combination of transpression and lateral extrusion (D3, Fig. 9) as proposed by Fritz et al. (2002). Presence of extensional and transcurrent ductile shears within WHC gives support for this conclusion. These shears cut across all of the above structures, hence, are late-stage structures (Fowler and El Kalioubi, 2002).

CONCLUSION

1. Documentation of ages and quantitative constraints on the pressure/temperature histories across the Wadi Hafafit Culmination (WHC) provides new insight into the tectono-metamorphic evolution of one of the key localities to understand the Neoproterozoic tectonometamorphic evolution in the Eastern Desert of Egypt.

2. Two distinct metamorphic phases have been recognized within WHC which are in agreement with petrogenetic grids for the observed assemblages. The first metamorphic phase (M1), equilibrated between 400 and 550°C and between 3.7 and 4.9 kbar, is observed in the micaschists of the Nugrus unit and is related to its thrusting over Hafafit unit (D2). The second metamorphic phase (M2), equilibrated in the range 600-750°C at 6-8 kbar, is observed in gneisses and amphibolites of the Hafafit unit and is related to the late D2 stage.

3. Sm/Nd dating of whole rock-garnet-plagioclase yields similar ages of ca. 590 Ma for Hafafit gneisses and amphibolite, which is interpreted as cooling from the thermal peak which was attained around 600 Ma or slightly earlier. A younger Rb-Sr of whole rock-biotite-plagioclase for biotite gneiss (573 ± 6 Ma) is interpreted as reflecting a later stage in the cooling history than the Sm-Nd ages.

4. The tectonic evolution of the WHC could be explained in three main stages: a) rifting and ocean floor spreading at a time earlier than 680 Ma; b) Subduction around 620-640 Ma. It was terminated by collision and nortwestward thrusting of the Nugrus unit over the Hafafit unit; and c) late-orogenic extension and crustal thinning that was controlled by the Najd transform faults that resulted in exhumation of the Hafafit domes through a combination of transpression and lateral extrusion.

ACKNOWLEDGMENTS

Our thanks are due to German Academic Exchange (DAAD) for supporting the post-doctoral visit of the first author at Tübingen University (Germany). We are grateful to M. El Ahmadi for supporting us with field facilities. Our thanks are also due to Th. Wenzel, Tübingen University, for his help with the electron microprobe analyses. Critical comments on the manuscript by M. Okrusch are gratefully acknowledged. Careful and insightful review of the manuscript by G. Pugnaire and M. Abu Anbar are gratefully acknowledged.

REFERENCES

Abd El-Naby, H., Frisch, W., 2002. Origin of Wadi Haimur-Abu Swayel gneiss belt, south Eastern Desert, Egypt: petrological and geochronological constraints. Precambrian Research, 113, 307-332.

Abd El-Naby, H., Frisch, W., 2006. Geochemical constraints from the Hafafit Metamorphic Complex (HMC): evidence of Neoproterozoic back-arc basin development in the central Eastern Desert of Egypt. Journal of African Earth Science, 45, 173-186.

Abd El-Naby, H., Frisch, W., Hegner, E., 2000. Evolution of Pan-African Wadi Haimur metamorphic sole, Eastern Desert, Egypt. Jounal of Metamorphic Geology, 18, 639-651.

Abdelsalam, M.G., Stern, R.J., 1993. Structure of the late Proterozoic Suture, Sudan. Journal of Geological Society of London, 150, 1065-1074.

Beaumont, C., Jamieson, R.A., Nguyen, M.H., Lee, B., 2001. Mid-crustal channel flow in large hot orogens: results from coupled thermal-mechanical models, in Slave - Northern Cordillera Lithospheric Evolution (SNORCLE) and Cordilleran Tectonics Workshop; Report of 2001 Combined Meeting, Lithoprobe Report, compiled by F. Cook and P. Erdmer, 112-170.

Bennett, J.D., Mosley, P.N., 1987. Tiered-tectonics and evolution, Eastern Desert and Sinai, Egypt. In: Matheis, G., Schandelmeier, H. (eds.). Current research in African earth sciences. Rotterdam, Balkema, 79-82.

Berhe, S.M., 1990. Ophiolites in northeast and east Africa: implications for Proterozoic crustal growth. Journal of Geological Society of London, 147, 41–51.

Berman, R.G., 1991. Thermobarometry using multi-equilibrium calculations: a new technique with petrological applications. Canadian Mineralogists, 29, 833-855.

Bhattacharya, A., Mohanty, L., Maji, A., Sen, S.K., Raith, M., 1992. Non-ideal mixing in the phlogopite-annite binary: constraints from experimental data on Mg-Fe partitioning and a reformulation of the biotite-garnet geothermometer. Contributions to Mineralogy and Petrology, 111, 87-93.

Blasband, B., Brooijmans, P., Dirks, P., Visser, W., White, S., 1997. A Pan-African core complex in the Sinai, Egypt. Geologie en Mijnbouw, 76, 247-266.

Blasband, B., White, S., Brooijmans, P., De Boorder, H., Visser, W., 2000. Late Proterozoic extensional collapse in the Arabian-Nubian Shield. Journal of Geological Society of London, 157, 615–628.

Bucher, K., Frey, M., 1994. Petrogenesis of metamorphic rocks. 6th Edition, Berlin, Springer, 341 pp.

Burchfiel, B.C., Royden, L.H., 1985. North-south extension within the convergent Himalayan region. Geology (Boulder), 13(10), 679-682.

Camp, V.E., 1984. Island arcs and their role in the evolution of the western Arabian Shield. Geological Society of America Bulletin, 95, 913-921.

Davidson, C., Grujic, D.E., Hollister, L.S., Schmid, S.M., 1997. Metamorphic reactions related to decompression and synkinematic intrusion of leucogranite, High Himalayan Crystalline, Bhutan. Journal of Metamorphic Geology, 15, 593-612.

Edwards, M.A., Kidd, W.S.F., Li, J., Yue,Y., Clark, M., 1996. Multi-stage development of the southern Tibet detachment system near Khula Kangri. New data from Gonto La. Tectonophysics, 260, 1-19.

El Gaby, S., El Nady, O., and Khudeir, A., 1984. Tectonic evolution of the basement complex in the central Eastern Desert of Egypt. Geologische Rundschau, 73, 1019-1036.

El Gaby, S., List, F. K., and Tehrani, R., 1988. Geology, evolution and metallogenesis of the Pan-African belt in Egypt. In: El Gaby, S., Greiling, R. O. (eds.) The Pan-African belt of northern Africa and adjacent areas. Vieweg, Braunschweig, 17-68.

El Ramly, M. F., Greiling, R., Kröner, A., Rashwan, A. A., 1984. On the tectonic evolution of the Wadi Hafafit area and environs, Eastern Desert of Egypt. Journal of King Abdulaziz University, Earth Sciences, 6, 113-126.

El Ramly, M.F., Greiling, R.O., Rashwan, A.A., Rasmy, A.H., 1993. Explanatory note to accompany the geological and structural maps of Wadi Hafafit area, Eastern Desert of Egypt. Geological Survey of Egypt, Paper No. 68.

Ernst, W.G., 1988. Tectonic history of subduction zones inferred from retrograde blueschist P-T paths. Geology, 16, 1081-1084.

Ferry, J.M., Spear, F.S., 1978. Experimental calibration of the partitioning of Fe and Mg between biotite and garnet. Contributions to Mineralogy and Petrology, 66, 113-117.

Fowler, A., El Kalioubi, B., 2002. The Migif-Hafafit gneissic complex of the Egyptian Eastern Desert: fold interference patterns involving multiply deformed sheath folds. Tectonophysics, 346, 247-275.

Fritz, H., Wallbrecher, E., Khudeir, A.A., Abu El Ela, F., Dallmeyer, R.D., 1996. Formation of Neoproterozoic metamorphic core complexes during oblique convergence (Eastern Desert, Egypt). Journal of African Earth Science, 23, 311–329.

Fritz, H., Dallmeyer, R.D., Wallbrecher, E., Loizenbauer, J., Hoinkes, G., Neumayr, P., Khudeir, A.A., 2002. Neoproterozoic tectonothermal evolution of the central Eastern Desert of Egypt: a slow velocity tectonic process of core complex exhumation. Journal of African Earth Science, 34, 137–155.

Gans, P.B., Mahood, G.A., Schermer, E., 1989. Synextensional magmatism in the Basin and Range Province:A case study from the eastern Great Basin: Geological Society of America, Special Paper 233, 53 pp.

Graham, C.M., Powell, R., 1984. A garnet-hornblende geothermometer: calibration, testing and application to the Pelona Schist, Southern California. Journal of Metamorphic Geology, 2, 13-31.

Greiling, R.O., Kröner, A., El Ramly, M.F., 1984. Structural interference patterns and their origin in the Pan-African basement of the southeastern Desert of Egypt. In: Kröner, A., Greiling, R.O. (eds.). Precambrian tectonics illustrated. Schweizerbart, Stuttgart, Germany, 401-412.

Greiling, R.O., Kröner, A., El Ramly M.F., Rashwan, A.A., 1988. Structural relationships between the southern and central parts of the Eastern Desert of Egypt: details of a fold and thrust belt. In: El-Gaby, S., Greiling, R.O. (eds.). The Pan-African belt of Northeast Africa and adjacent areas. Germany, Vieweg publisher, Wiesbaden-Braunschweig, 121-146.

Greiling, R.O., Abdeen, M.M., Dardir, A.A., El Akhal, H., El Ramly, M.F., Kamal El Din, G.M., Osman, A.F., Rashwan, A.A., Rice, A.H.N., Sadek, M.F., 1994. A structural synthesis of the proterozoic Arabian –Nubian shield in Egypt. Geologisches Rundschau, 83, 484-501.

Guidotti, C.V., Sassi, F.P., 1976. Muscovite as a petrogenetic indicator mineral in pelitic schists. Neues Jahrbuch für Mineralogie, 127, 97-142.

Hashad, A.H., Sayyah, T.A., El Manharawy, M.S., 1981. Isotopic composition of strontium and origin of Wadi Kareim volcanics, Eastern Desert. Egyptian Journal of Geology, 25, 141-147.

Hey, M.A., 1954. A review of the chlorites. Mineralogical Magazine, 30, 277-292.

Hodges, K.V., Spear, F.S., 1982. Geothermometry, geobarometry and the Al_2SiO_5 triple point at Mt. Moosilauke, New Hampshire. American Mineralogist, 67, 1118-1134.

Holland, T.J.B., Blundy, J., 1994. Non-ideal interactions in calcic amphiboles and their bearing on amphibole-plagioclase thermometry. Contributions to Mineralogy and Petrology, 116, 433–447.

Hynes, A., Forest, R.C., 1988. Empirical garnet-muscovite geothermometry in low-grade metapelites, Selwyn range (Canadian Rockies). Journal of Metamorphic Geology, 6, 297-309.

Johnson, P.R., Vranas, G.J., 1984. The origin and development of Late Proterozoic rocks of the Arabian Shield. DGMR. Jeddah Open-File Report, 4-32.

Kleemann, J., Reinhardt, J., 1994. Garnet-biotite thermometry revisited: The effect of Al(VI) and Ti in biotite. European Journal of Mineralogy, 6, 925-941.

Kohn, M.J., Spear, F.S., 1990. Two new geobarometers for garnet amphibolites, with applications to southern Vermont. American Mineralogist, 75, 89-96.

Kretz, R., 1983. Symbols for rock-forming minerals. American Mineralogist, 68, 277–279.

Kröner, A., Todt, W., Hussein, I.M., Mansour, M., Rashwan, A.A., 1992. Dating of late Proterozoic ophiolites in Egypt and Sudan using the single grain zircon evaporation technique, Precambrian Research, 59, 15-32.

Leake, B.E., Woolley, A.R., Arps, C.E.S., Birch, W.D., Gilbert, M.C., Grice, J.D., Hawthorne, F.C., Kato, A., Kisch, H.J., Krivovichev, V.G., Linthout, K., Laird, J., Mandarino, J.A., Maresch, W.V., Nickel, E.H., Rock, N.M.S., Schumacher, J.C., Smith, D.C., Stephenson, N.C.N., Ungaretti, L., Whittaker, E.J.W., Youzhi, G., 1997. Nomenclature of amphiboles: Report of the Subcommittee on Amphiboles of the International Mineralogical Association, Commission on New Minerals and Mineral Names. Mineralogical Magazine, 61, 295–321.

Liew, T.C. Hofmann, A.W., 1988. Precambrian crustal components, plutonic associations, plate environment of the Hercynian fold belt of central Europe: Indications from an Nd and Sr isotopic study. Contrib. Mineral. Petrol., 98, 129-138.

Lister, G.S., Baldwin S.L., 1993. Plutonism and the origin of metamorphic core complexes. Geology, 21, 607-610.

Loizenbauer, J., Wallbrecher, E., Fritz, H., 1999. The Deformation History of the Meatiq Metamorphic Core Complex, Eastern Desert, Egypt: Constraints on Geochronology, Structural Analyses and Fluid Inclusion Studies. Journal of Conference Abstracts, 4(1), Session A05:5A, p. 1.

Loizenbauer, L., Wallbrecher, E., Fritz, H., Neumayr, P., Khudeir, A.A., Kloetzli, U., 2001. Structural Geology, single zircon ages and fluid inclusion studies of the Meatiq metamorphic core complex: Implications for Neoproterozoic tectonics in the Eastern Desert of Egypt. Precambrian Research, 110, 357-383.

Mancktelow, N.S., 1995. Nonlithostatic pressure during sediment subduction and the development and exhumation of high pressure metamorphic rocks. Journal of Geophysical Research, 100, 571-583.

Massonne, H.J., Schreyer, W., 1987. Phengite geobarometry based on the limiting assemblage with K-feldspar, phlogopite and quartz. Contributions to Mineralogy and Petrology, 96, 212-224.

Mezger, K., Essene, E.J., Halliday, A.N., 1992. Closure temperature of the Sm/Nd system in metamorphic garnets. Earth Planetary Science Letter, 113, 397-409.

Moghazi, A.M., Hassanen, M.A., Mohamed, F.H., Ali, S., 2004. Late Neoproterozoic strongly peraluminous leucogranites, South Eastern desert, Egypt: petrogenesis and geodynamic significance. Mineralogy and Petrology, 81, 19-41.

Neumayr, P., Mogessie, A., Hoinkes, G., Puhl, J., 1996. Geological setting of the Meatiq metamorphic core complex in the Eastern Desert of Egypt based on amphibolite geochemistry. Journal of African Earth Science, 23, 331-345.

Neumayr, P., Hoinkes, G., Puhl, J., Mogessie, A., Khudier, A.A., 1998. The Meatiq dome (Eastern Desert, Egypt) a Precambrian metamorphic core complex: petrological and geological evidence. Journal of Metamorphic Geology, 16, 259-279.

Stern, R.J., Hedge, C.E., 1985. Geochronologic and isotopic constraints on Late Precambrian crustal evolution in the Eastern Desert of Egypt. American Journal of Sciences, 285, 97-127.

Stern, R.J., 1985. The Najd Fault System, Saudi Arabia and Egypt: a late Precambrian rift related transform system? Tectonics, 4, 497-511.

Stoeser, D.B., Camp, V.E., 1985. Pan-African microplate accretion of the Arabian Shield. Geological Society of America Bulletin, 96, 817-826

Velde, B., 1967. Si^{4+} content of natural phengites. Contributions to Mineralogy and Petrology, 17, 250-258.

Wendt, I., 1986. Radiometrische Methoden in der Geochronologie. Clausthaler Tektonische Hefte 23, Pilger, Clausthal Zellerfeld, 170 pp.

Manuscript received October 2007;
revision accepted April 2008;
published Online October 2008.

TABLE 1 | **Sequence of structural events for the WHC, as proposed by Greiling et al. (1984), El Ramly et al. (1993), Greiling et al. (1994) and Fowler and El Kalioubi (2002).**

Greiling et al. (1984)	El-Ramly et al. (1993)		Greiling et al. (1994)		Fowler and El Kalioubi (2002)
''Early deformation''	D1	planar fabric	D1	planar fabric	progressively more silicic calc-alkaline syn-kinematic intrusions gneissosity and lineations isoclinal folds, macroscopic sheath folds mylonites
	D2	metamorphic banding, migmatization	D2	metamorphic banding, migmatization	
	D3	foliation, isoclinal folds	D3	foliation, isoclinal folds	
	D4	foliation, isoclinal folds	D4	foliation, isoclinal folds	
''Early thrusting and folding''	D5	mylonites	D5	mylonites	
	D6	NE–SW trending fault bend folds	D6	NE–SW trending open folds	NE–SW trending upright open folds macroscopic monoclinal folds
	D7	drag folds	D7	drag folds	thrusting
''Regional thrusting and folding''	D8	thrusting	D8	thrusting mylonites fault bend folds	
	D9	chevron folds			
	D10	NW–SE trending open folds			NW–SE trending upright folds
''Gravitative uplift''	D11	open folds, flat-lying axial surfaces	D9	open folds, flat-lying axial surfaces	not present

Data from Fowler and El Kalioubi (2002)

TABLE 2 | **Mineral assemblages of the studied samples.**

Sample	Hbl*	Pl	Grt	Qtz	Cpx	Bt	Chl	Ms	Zrn	Ilm
H17 (Garnet amphibolite)	x	x	x	x	x					x
H19, H4 (Garnet amphibolites)	x	x	x	x						x
H11, H21, H14 (Cpx-amphibolites)	x	x		x	x					x
H8, H24, H23 (Bt-Hbl-gneisses)	x	x		x		x				x
H18, H2, H16 (Bt-Hbl-gneisses)	x	x	x	x		x	x		x	
N10 (Micaschist)		x	x	x		x	x	x		x
N21, N22, N23 (Micaschists)		x	x	x		x		x		x

*Mineral Abbreviation after Kretz (1983).

TABLE 3 | **Representative electron microprobe analyses of amphibole.**

	Garnet amphibolites			Cpx-amphibolites			Bt- and Hbl-gneisses	
Sample	H17	H19	H4	H11	H14	H21	H8	H24
	(N=6)	(N=6)	(N=6)	(N=5)	(N=6)	(N=6)	(N=6)	(N=7)
SiO_2	45.18	47.08	43.92	48,00	48,00	47.12	45.9	43.74
TiO_2	0.84	0.75	0.97	0.48	0.62	0.38	1.04	1.00
Al_2O_3	10.79	9.8	13.17	8.23	6.98	11.22	10.54	11.63
FeO*	14.17	14.12	17.98	11.68	16.95	8.04	13.31	14.69
MnO	0.11	0.11	0.17	0.19	0.3	0.14	0.24	0.41
MgO	11.97	12.59	9.21	14.45	11.07	15.94	12.53	11.73
CaO	11.28	11.06	10.93	12.32	12.06	12.73	11.61	11.42
Na_2O	1.41	0.98	1.25	0.99	0.64	1.72	1.23	1.27
K_2O	0.68	0.25	0.51	0.28	0.45	0.43	0.4	0.42
Total	96.43	96.74	98.11	96.62	97.07	97.72	96.8	96.31
				Cations per 23 oxygen				
Si	6.73	6.93	6.53	7.01	7.21	6.76	6.77	6.63
Ti	0.09	0.08	0.11	0.05	0.07	0.04	0.12	0.11
Al	1.89	1.7	2.31	1.43	1.24	1.9	1.83	2.08
Fe^{2+}	1.77	1.74	2.24	1.44	2.13	0.96	1.64	1.86
Mn	0.01	0.01	0.02	0.02	0.04	0.02	0.03	0.05
Mg	2.66	2.76	2.04	3.18	2.48	3.41	2.76	2.65
Ca	1.8	1.74	1.74	1.95	1.94	1.96	1.84	1.85
Na	0.41	0.28	0.36	0.28	0.19	0.48	0.35	0.37
K	0.13	0.05	0.1	0.05	0.09	0.08	0.08	0.08
Total	15.49	15.29	15.45	15.41	15.39	15.61	15.42	15.68

N: number of analyses. * Total Fe as FeO.

TABLE 4 | **Representative electron microprobe analyses of plagioclase.**

	Garnet amphibolites			Cpx amphibolites			Bt- and Hbl-gneisses					Micaschists	
Sample	H17	H19	H4	H11	H21	H14	H8	H24	H18	H2	H16	N21	N10
	(N=6)	(N=9)	(N=8)	(N=8)	(N=10)	(N=5)	(N=5)	(N=8)	(N=7)	(N=10)	(N=28)	(N=6)	(N=9)
SiO_2	58.34	50.35	60.59	51.2	53.06	60.23	58.47	60.01	62,00	61.46	65.63	64.08	65,00
Al_2O_3	23.97	31.89	25.17	30.35	28.95	25.17	26.36	25.71	23.74	24.06	21.87	22.58	21.67
FeO*	0.31	0.14	0.17	0.58	0.6	0.46	0.16	0.07	0.08	0.07	0,00	0.07	0.02
CaO	9.33	15.55	7.48	13.23	11.66	7.7	8.68	8.09	6.18	6.56	3.53	3.56	3.04
Na_2O	7.1	2.67	7.28	2.82	4.88	7.06	6.55	6.92	8.1	7.49	9.3	9.43	9.79
K_2O	0.21	0.03	0.03	1.04	0.05	0.09	0.07	0.12	0.17	0.33	0.28	0.1	0.15
Total	99.26	100.6	100.7	99.22	99.2	100.71	100.2	100.9	100.6	99.98	100.6	99.81	100,0
						Cations per 8 oxygen							
Si	2.65	2.28	2.68	2.35	2.43	2.67	2.61	2.65	2.75	2.73	2.87	2.83	2.87
Al	1.28	1.7	1.31	1.64	1.56	1.31	1.38	1.34	1.24	1.26	1.13	1.17	1.12
Fe^{2+}	0.01	0.01	0.01	0.02	0.02	0.02	0.01	0,00	0,00	0,00	0,00	0,00	0,00
Ca	0.45	0.76	0.35	0.65	0.57	0.37	0.42	0.38	0.29	0.31	0.17	0.17	0.14
Na	0.63	0.24	0.62	0.25	0.43	0.61	0.57	0.59	0.7	0.65	0.79	0.81	0.84
K	0.01	0,00	0,00	0.06	0,00	0.01	0,00	0.01	0.01	0.02	0.02	0.01	0.01
Total	5.03	4.99	4.97	4.97	5.01	4.99	4.99	4.97	4.99	4.97	4.98	4.99	4.98
						Molar proportion							
Or	1.1	0.2	0.2	6.3	0.3	0.5	0.4	0.6	0.9	1.9	1.6	0.6	0.8
Ab	57.3	23.7	63.7	26.1	42.9	62.1	57.5	60.4	69.7	66.1	81.3	82.3	84.7
An	41.6	76.1	36.1	67.6	56.8	37.4	42.1	39,00	29.4	32,00	17,00	17.1	14.5

N: number of analyses. * Total Fe as FeO. Or. orthoclase; Ab. albite; An. anorthite.

TABLE 5 | **Representative electron microprobe analyses of garnet.**

	Garnet amphibolites			Bt-gneisses		Micaschists		
Sample	H17 (N=7)	H19 (N=12)	H4 (N=13)	H16 (N=5)	H18 (N=10)	N10 (N=9)	N22 (N=10)	N23 (N=13)
SiO_2	38.66	37.24	37.61	37.17	36.41	36.96	36.12	37.87
TiO_2	0.08	0.04	0,00	0.047	0,00	0.08	0.09	0.06
Al_2O_3	20.93	20.99	20.96	20.46	21.32	20.93	21.12	20.79
Cr_2O_3	0.48	0.02	0,00	0.368	0.15	0.05	0.03	0,00
FeO*	24.86	27.39	31.31	34.61	31.33	39.81	28.12	27.3
MnO	1.08	1.2	0.9	1.42	5.94	0.13	6.43	5.6
MgO	4.44	3.79	3.04	2.04	3.21	1.16	0.13	0.98
CaO	9.94	8.69	5.9	3.26	1.87	0.4	7.55	7.94
Na_2O	0.04	0.04	0,00	0.065	0.02	0.09	0.13	0,00
Total	100.5	99.39	99.73	99.44	100.25	99.6	99.72	100.53
				Cations per 12 oxygen				
Si	3.01	3,00	3.01	3.02	2.92	3.03	2.93	3.03
Ti	0.01	0,00	0,00	0,00	0,00	0.01	0.01	0,00
Al	1.92	1.99	1.97	1.96	2.02	2.02	2.02	1.96
Cr	0.03	0,00	0,00	0.02	0.01	0,00	0,00	0,00
Fe^{2+}	1.62	1.91	2.09	2.35	2.1	2.73	1.91	1.83
Mn	0.07	0.08	0.06	0.1	0.4	0.01	0.44	0.38
Mg	0.52	0.46	0.36	0.25	0.38	0.14	0.02	0.12
Ca	0.83	0.75	0.51	0.28	0.16	0.04	0.66	0.68
Na	0.01	0.01	0,00	0.01	0,00	0.01	0.02	0,00
Total	8.02	8.2	8,00	7.99	7.99	7.99	8.01	8,00
				Molar proportion**				
Alm	53.26	56.93	69.27	78.9	68.85	93.6	63.1	60.8
Prp	16.96	15.16	12,00	8.3	12.59	4.9	0.5	3.9
Grs	25.76	15.89	16.72	9.5	4.77	1.2	21.7	22.7
Sps	2.33	2.73	2.01	3.3	13.22	0.3	14.7	12.64

N: number of analyses. * Total Fe as FeO. ** Alm: almandine; Prp: pyrope; Grs: grossular; Sps: spessartine.

TABLE 6 | **Representative electron microprobe analyses of clinopyroxene.**

	Cpx-amphibolites		
Sample	H11 (N=11)	H14 (N=9)	H21 (N=13)
SiO_2	53.49	53.63	53.29
TiO_2	0.04	0.02	0.04
Al_2O_3	0.55	0.32	0.63
Cr_2O_3	0.03	0.00	0.00
FeO*	6.74	6.29	6.83
MnO	0.3	0.3	0.29
MgO	14.32	14.58	14.34
CaO	24.54	24.83	24.62
Na_2O	0.24	0.14	0.22
Total	100.25	100.11	100.26
	Cations per 6 oxygen		
Si	1.98	1.98	1.98
Ti	0.00	0.00	0.00
Al	0.02	0.01	0.03
Cr	0.00	0.00	0.00
Fe^{2+}	0.21	0.2	0.21
Mn	0.01	0.01	0.01
Mg	0.79	0.8	0.79
Ca	0.97	0.98	0.96
Na	0.02	0.01	0.02
Total	4.00	3.99	4.00

N: number of analyses. * Total Fe as FeO.

TABLE 7 | **Representative electron microprobe analyses of biotite.**

	Bt-gneisses		Micaschists		
Sample	H16 (N=7)	H18 (N=13)	N10 (N=11)	N22 (N=8)	N23 (N=6)
SiO_2	34.79	35.37	33.89	33.31	34.94
TiO_2	0.019	0.62	1.53	2.96	2.79
Al_2O_3	19.08	18.91	19.32	18.75	18.35
FeO*	21.88	20.53	27.38	26.3	22.65
MnO	0.41	0.24	0.05	0.11	0.29
MgO	9.97	10.28	4.04	3.36	6.94
CaO	0.33	0.04	0.13	0.14	0.11
Na_2O	0.19	0.06	0.13	0.09	0.07
K_2O	9.67	9.21	8.95	9.2	9.36
Cl	0.03	0.01	0.02	0,00	0.01
Total	96.37	95.27	95.43	94.22	95.52
		Cations per 22 oxygen			
Si	5.57	5.66	5.6	5.58	5.65
Ti	0.002	0.07	0.19	0.37	0.34
Al	3.6	3.56	3.76	3.7	3.5
Fe^{2+}	2.93	2.75	3.78	3.68	3.06
Mn	0.06	0.03	0.01	0.02	0.04
Mg	2.38	2.45	1,00	0.84	1.67
Ca	0.06	0.01	0.02	0.02	0.02
Na	0.06	0.02	0.04	0.03	0.02
K	1.98	1.88	1.89	1.96	1.93
Total	16.64	16.43	16.29	16.2	16.23
(Mg/(Mg+Fe)	0.45	0.47	0.21	0.19	0.35

N: number of analyses. * Total Fe as FeO.

TABLE 8 | **Representative analyses of muscovite and chlorite in micaschists.**

Sample	Muscovite N10 (N=10)	Muscovite N22 (N=10)	Muscovite N23 (N=13)	chlorite N22 (N=7)
SiO_2	48.99	49.2	48.14	24.37
TiO_2	0.45	0.52	0.34	0.16
Al_2O_3	36.33	35.56	35.95	19.72
FeO*	1.48	1.46	1.41	39.89
MnO	0.02	0.03	0.04	0.45
MgO	0.68	0.54	0.74	2.29
CaO	0.02	0.04	0.01	0.1
Na_2O	0.33	0.28	0.34	0.00
K_2O	10.57	10.62	10.97	0.55
Total	98.87	98.25	97.94	87.53
	Cations per 22 oxygen for muscovite			
	Cations per 28 oxygen for chlorite			
Si	6.54	6.61	6.51	5.62
Ti	0.05	0.05	0.04	0.03
Al	5.71	5.62	5.73	5.35
Fe^{2+}	0.17	0.16	0.16	7.69
Mn	0.00	0.00	0.01	0.09
Mg	0.14	0.11	0.15	0.79
Ca	0.00	0.01	0.00	0.03
Na	0.09	0.07	0.09	0.00
K	1.8	1.82	1.89	0.16
Total	14.5	14.45	14.58	19.76

N: number of analyses. * Total Fe as FeO.

TABLE 9 | **Calculated temperatures and pressures for the Hafafit rocks.**

	Nugrus unit			Hafafit unit								
	Micaschists			Garnet-amphibolites			Cpx-amphibolites			Bt- and Hbl-gneisses		
	N10	N22	N23	H19	H17	H4	H11	H21	H14	H8	H24	H18
Grt-Bt geothermo-meter T (°C)												
Bhattacharya et al. (1992)	465-515		405-454									598-622
Ferry and Spear (1978)	470-535		435-500									628-665
Hodges and Spear (1982)	477-540		515-550									650-686
Kleemann and Reinhardt (1994)	517-535		519-521									617-622
Grt-Am geothermometer T (°C)												
Graham &Powell (1984)				600-607	665- 713	650-750						
Hbl-Pl geothermometer T (°C)												
Holland and Blundy (1994)				689-690	635-651	657-682	700-712	720-750	662-682	660-730	720-730	
Grt -Ms geothermometer T (°C)												
Hynes and Forest (1988)	424-508	400-447	466-527									
Grt - Hbl-Pl -Qtz geobarometer P (kb)												
Kohn and Spear (1990)				6.0– 6.5	7.6 - 8.0	6.5– 7.6						
White mica geobarometer P (kb)												
Massonne and Schreyer (1987)	4.3 - 4.9	3.7– 4.3	4.0– 4.8									
TWEEQU T (°C)												
Berman (1991)	480-550		465-527									

TABLE 10 | **Rb-Sr and Sm-Nd isotopic composition (in ppm).**

Rb-Sr isotopic composition

Sample	Age (Ma)	Type	Sr	Rb	$^{87}Rb/^{86}Sr$	$^{87}Sr/^{86}Sr$	$^{87}Sr/^{86}Sr$ (i)	_Sr(T)
H18	573	WR	113.5	26.67	0.6802	0.710201	0.70464	12
H18	573	biotite	13.63	213.6	47.039	1.088207	0.70391	1
H18	573	Plg	233.7	14.25	0.1764	0.705727	0.70429	7

Sm-Nd isotopic composition*

Sample	Age (Ma)	Type	Sm	Nd	$^{147}Sm/^{144}Nd$	$^{143}Nd/^{144}Nd$	$^{143}Nd/^{144}Nd$(i)	eNd(T)	eNd(0)	TDM*
H23	593	WR	0.443	1.413	0.1894	0.512916	0.512180	6.0	5.4	0.78
H23	593	Granat	0.692	0.292	1.4352	0.517749	0.512172	5.8	99.7	0.80
H23	593	Plg	0.087	0.656	0.0798	0.512485	0.512175	5.9	-3.0	0.79
H19	585	WR	1.090	3.402	0.1938	0.512877	0.512134	4.9	4.7	0.87
H19	585	Granat	0.162	0.173	0.5686	0.514298	0.512118	4.6	32.4	0.89
H19	585	Plg	0.197	1.296	0.0917	0.512466	0.512114	4.5	-3.4	0.90

* model age after Liew and Hofmann (1988).